

Dissecting Fragment-Based Lead Discovery at the von Hippel-Lindau Protein:Hypoxia Inducible Factor 1 α Protein-Protein Interface

Inge Van Molle,¹ Andreas Thomann,¹ Dennis L. Buckley,² Ernest C. So,¹ Steffen Lang,¹ Craig M. Crews,^{2,3,4} and Alessio Ciulli^{1,*}

¹Department of Chemistry, University of Cambridge, Cambridge, CB2 1EW, UK

²Department of Chemistry

³Department of Molecular, Cellular and Developmental Biology

⁴Department of Pharmacology

Yale University, New Haven, CT 06511, USA

*Correspondence: ac313@cam.ac.uk

<http://dx.doi.org/10.1016/j.chembiol.2012.08.015>

SUMMARY

Fragment screening is widely used to identify attractive starting points for drug design. However, its potential and limitations to assess the tractability of often challenging protein:protein interfaces have been underexplored. Here, we address this question by means of a systematic deconstruction of lead-like inhibitors of the pVHL:HIF-1 α interaction into their component fragments. Using biophysical techniques commonly employed for screening, we could only detect binding of fragments that violate the Rule of Three, are more complex than those typically screened against classical druggable targets, and occupy two adjacent binding subsites at the interface rather than just one. Analyses based on ligand and group lipophilicity efficiency of anchored fragments were applied to dissect the individual subsites and probe for binding hot spots. The implications of our findings for targeting protein interfaces by fragment-based approaches are discussed.

INTRODUCTION

Protein-protein interactions (PPIs) are attractive targets for the development of small molecule chemical probes and drugs. However, targeting protein-protein interfaces with drug-like small molecules of desired potency and physicochemical properties has remained a formidable challenge (Yin and Hamilton, 2005; Wells and McClendon, 2007). Some successes have been achieved by targeting deep grooves on proteins that accommodate alpha helical motifs; however, shallow and featureless interfaces that lack buried pockets have been traditionally harder to target. Although “hot spots” can be identified on either surface involved in the PPI by site-directed mutagenesis, these do not necessarily translate to hot spots for small molecule binding. In fact, binding small molecules solely to such hot spots does not always provide sufficient affinity for biological activity (Wells and McClendon, 2007; Kozakov et al.,

2011). Furthermore, many interfaces appear to be highly adaptable in their ability to bind to different protein partners, often using hidden cryptic pockets, but it is not well understood how best to exploit these features for drug design. Because the number and nature of protein-protein interactions successfully targeted with small molecules has remained limited, it is important to assess their tractability by discovering and properly characterizing new “druggable” or “ligandable” binding sites (Hajduk et al., 2005; Edfeldt et al., 2011; Fauman et al., 2011; Surade and Blundell, 2012).

Fragment-based lead discovery (FBLD) is firmly established as a powerful and efficient way to develop small molecule binders of desired potency and physicochemical properties, with notable successes targeting enzyme active sites (Erlanson et al., 2004; Hajduk and Greer, 2007; Congreve et al., 2008; Murray and Rees, 2009). There is increasing hope that FBLD may provide new solutions to address difficult targets, including PPIs, in part because of the limited success of more traditional methods, including high-throughput screening (HTS), against these difficult targets (Coyne et al., 2010; Crews, 2010). The higher hit rates in screening, higher ligand efficiencies, and greater sampling of chemical space that are afforded by smaller fragments compared to larger compounds present in HTS libraries are among the key features that make fragment-based approaches highly attractive, provided that weak binding interactions can be reliably detected (Ciulli and Abell, 2007). Fragment screens are therefore typically performed experimentally using sensitive biophysical techniques, such as NMR spectroscopy, fluorescence-based and thermal methods, surface plasmon resonance, and X-ray crystallography, or computationally using molecular docking (Ciulli et al., 2006; Teotico et al., 2009; Larsson et al., 2011). On the other hand, some have posited that nontraditional pharmaceutical targets, such as PPIs, would be unlikely to be suitable for FBLD, partly because the small aromatic fragments that enrich typical fragment libraries would be expected to bind poorly to the flat, more solvent exposed, and often dynamic protein surfaces (Hajduk et al., 2011). Although this may seem a problem primarily of library design, druggable pockets that would be suitable to accommodate binding of small molecular fragments have indeed shown to be either too small in size to achieve desired level of binding affinities (Maurer et al., 2012; Sun et al., 2012) or highly cryptic, often

exhibiting a degree of plasticity that could only be explored by covalent tethering (Erlanson et al., 2000), serendipitously (Śledź et al., 2011), or by targeting mutational cavities (Basse et al., 2010). Nevertheless, a few successes have been achieved by targeting PPIs using fragment screening, such as in the cases of the anticancer Bcl target family (Petros et al., 2006), interleukins (Braisted et al., 2003), and the ZipA/FtsZ interaction (Tsao et al., 2006). Many more examples will likely be reported in future years, given the interest and promise of this area. However, the field is still in its infancy, and the question of whether FBLD will ultimately deliver more successes and compounds of better physicochemical properties than other approaches to date remains unanswered.

It was first observed by Wells and McClendon (2007) that high-affinity inhibitors of PPIs, irrespective of the approach being used to discover them, tend to have, on average, significantly lower ligand efficiencies (LE ~ 0.24 kcal mol⁻¹ NHA⁻¹, defined as binding energy relative to number of heavy atoms NHA)

$$LE = \frac{-\Delta G}{NHA} = \frac{-RT \ln K_d}{NHA}$$

(Hopkins et al., 2004) when compared with compounds targeting enzyme active sites (LE ~ 0.3 – 0.4 kcal mol⁻¹ NHA⁻¹) (Wells and McClendon, 2007). Small molecules targeting PPIs that were discovered by several approaches, including FBLD, have been analyzed and found to be larger in size, to have higher lipophilicity (as measured by CLogP), and to contain more rings and fewer rotatable bonds on average than those for drugs and ligands targeting active sites (Higuero et al., 2009; Morelli et al., 2011). These in turn will likely result in poorer physicochemical and pharmacological properties, including lower solubility, poorer cell permeability, and nonspecific toxicity (Leeson and Springthorpe, 2007). Therefore, not only it is important to identify druggable hot spots at protein interfaces, it is also crucial to evaluate their ability to yield high-affinity ligands while keeping molecular weight and lipophilicity under control. For these purposes, a metric called ligand lipophilic efficiency

$$LLE_{AT} = 0.11 + RT \ln(10) \frac{pK_d - cLogP}{NHA}$$

has been recently introduced by Astex Pharmaceuticals in order to scale binding affinities by both size and lipophilicity in a manner consistent with LE, thus enabling control of each property during optimization (Mortenson and Murray, 2011). However, this metric has not been extensively used to date when assessing the ligandability of PPIs.

Here, we present a rigorous deconstructive fragment-based study to probe the tractability of a model protein-protein interface, that is, between the von Hippel-Lindau protein (pVHL) and the alpha subunit of hypoxia-inducible factor 1 (HIF-1 α) (Jaakkola et al., 2001; Hon et al., 2002; Min et al., 2002). pVHL is the substrate binding module of the VHL Cullin RING type E3 ubiquitin ligase (CRL2^{VHL}), a multi-subunit complex composed also of Elongin B, Elongin C, Cullin-2, and Rbx1. pVHL functions to direct proteasomal degradation of HIF-1 α under high oxygen conditions; its critical role in cellular oxygen sensing and the hypoxic response are well established, whereas many noncanonical HIF-independent roles remain to be elucidated (Jaakkola et al., 2001; Kaelin, 2008). The pVHL:HIF-1 α interaction involves

recognition of a long, flexible region of HIF-1 α and of a key post-translational modification (proline hydroxylation). We recently reported the computational design of lead-like small molecule inhibitors of this PPI that mimic the structure of the HIF-1 α peptide (Buckley et al., 2012). This provided the starting point for a model study to ask: could we have discovered these inhibitors using FBLD? What is the minimal complexity of fragments of the inhibitors required to detect their binding? Can “hot spots” for preferential fragment targeting be identified at the protein interface? In order to answer these questions, we structurally and biophysically characterized three pVHL binders and modularly fragmented them. Fragment binding was assessed using biophysical methods widely employed in fragment screening. Furthermore, we dissected the contribution of different groups to the ligand binding free energy by applying ligand and group lipophilicity efficiency metrics.

RESULTS

Crystal Structures of pVHL with Bound Small Molecule Inhibitors

Crucial to a fragment-based deconstructive analysis of small molecules targeting PPIs is the structural elucidation of the ligand binding modes. We solved cocrystal structures of the ternary complex pVHL-ElonginC-ElonginB (VCB, Figure 1A) with a 19-amino-acid-long peptide from HIF-1 α bound (Figure 1B; Figure S1 available online; see also Hon et al., 2002; Min et al., 2002) and with three bound inhibitors that we recently designed based on in silico modeling (1, Figure 1D; 2, Figure 1E; and 3, Figure 1C [Buckley et al., 2012]; see also Figure 3A). The structures revealed that the inhibitors fit snugly at the pVHL surface and mimic many of the key interactions observed in the pVHL:HIF-1 α structure. The targeted binding site can be schematically divided into three subsites: left-hand side (LHS), central core, and right-hand side (RHS) (Figure 1A). The central subsite is formed by several buried, mostly aromatic, residues of pVHL, namely, W88, Y98, H110, S111, H115, and W117, many of which are frequently mutated in VHL disease and sporadic renal cell carcinomas (Kaelin, 2008). This subsite recognizes *trans*-4-hydroxyproline (Hyp) in the most favored C⁴-*exo* conformation of its pyrrolidine ring, with the Hyp hydroxyl group forming two key hydrogen bonds to the side chains of H115 and S111 and replacing a water molecule bound at this position in the apo structure (Figure S1A) (Loenarz et al., 2009). In addition, hydrogen bonds are present between the carbonyl oxygen and the Y98 OH group and between the amide NH and the His110 carbonyl. The ligands recapitulate the key interactions observed between pVHL and Hyp564 of the HIF-1 α binding epitope. The LHS pocket is formed by two hydrophobic residues (F91 and Y112) and three hydrophilic amino acids (H115, N67, and R69). In addition, the LHS pocket contains a conserved water molecule that is seen in all four structures. The crystal structures show that the ligands' LHS isoxazole group forms a π - π interaction with the Y112 side chain and hydrogen bonds to this conserved water molecule, thereby recapitulating the interaction made by the HIF-1 α peptide epitope as a bioisostere of the Leu562 carbonyl. The RHS subsite is an elongated pocket defined mainly by hydrophobic amino acids, both at its entry (I109, F76, Y98, and W117) as well as further away from the

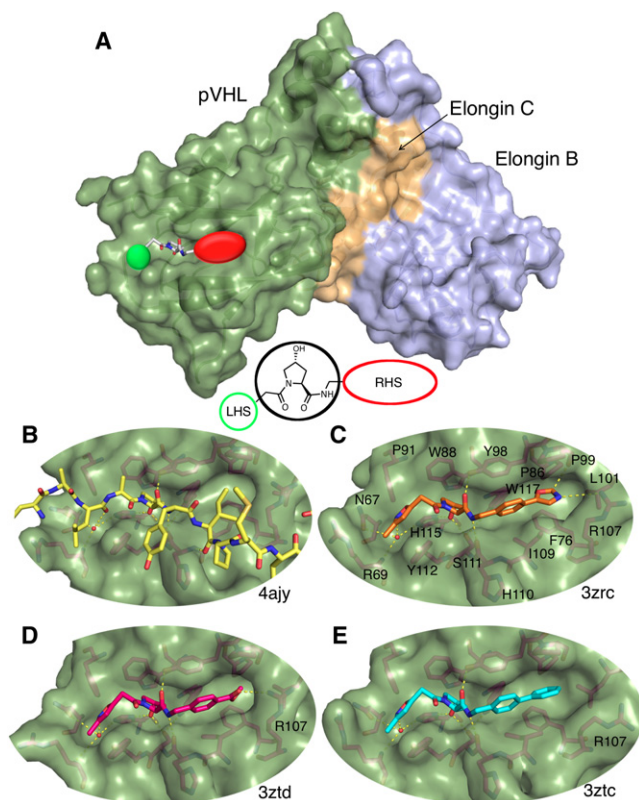


Figure 1. Structural Characterization of Small Molecules Targeting the pVHL:HIF-1 α Interactions

(A) General binding mode of small molecule inhibitors of pVHL:HIF-1 α , based on the crystal structure of the VCB ternary complex with **1** bound, as shown in (D). The small molecule is shown in stick representation, the left-hand side (LHS) and right-hand side (RHS) groups are shown as green and red spheres, respectively, as represented in the model structure below. VCB is shown in surface representation (pVHL in green, Elongin C in gold, and Elongin B in purple).

(B–E) Crystal structures of VCB in complex with a 19-mer HIF-1 α peptide (DEALAHypYIPMDDDFQLRSF) (**B**), **3** (**C**), **1** (**D**), and **2** (**E**) are shown with the ligands as stick representation bound on the surface of pVHL (green). Residues in the HIF-1 α binding site of pVHL are shown in magenta in stick representation. Residues are labeled in (C).

See also Figure S1 and Table S1.

central core (P86, P99, L101, and R107). The crystal structures show that the ligands' phenyl rings are involved in a side-on interaction with the Y98 phenol. A comparison of the bound structures of **1–3** demonstrates a degree of the plasticity of the RHS pocket of pVHL. The R107 side chain moves out to accommodate larger hydrophobic RHS substituents, as in the case of the biphenyl group of **2** (Figure 1E). Unlike in the case of **2**, the RHS oxazole group of **3** hydrogen bonds to the R107 NH2 as does the *p*-methylester group of **1** (Figures 1C–1D). In addition the CH at position **2** of the oxazole ring of **3** is hydrogen bonded to the P99 backbone carbonyl.

Biophysical Characterization of Inhibitors of the pVHL:HIF-1 α Interaction

To characterize fully the binding of the inhibitors to VCB, we employed four different biophysical techniques:

- (1) Differential scanning fluorimetry (DSF) to monitor protein thermal shifts in the presence of the dye Sypro Orange due to ligand-induced protein stabilization (Kranz and Schalk-Hihi, 2011);
- (2) One-dimensional ligand-observed ^1H NMR spectroscopy, including STD (Mayer and Meyer, 1999) and Water-LOGSY (Dalvit et al., 2001) experiments that monitor changes in ligand signals in the presence of protein due to cross-relaxation, after selective excitation of protein or water signals, respectively, and relaxation-edited Carr-Purcell-Meiboom-Gill (CPMG) experiments that allow monitoring of broadened bound ligand signals in the presence of the protein;
- (3) A fluorescence polarization (FP) assay to monitor the concentration-dependent displacement of the fluorescent HIF-1 α peptide, FAM-DEALAHypYIPD ($K_d = 560$ nM by FP) (Buckley et al., 2012); and
- (4) Isothermal titration calorimetry (ITC) to directly monitor the thermodynamic parameters of ligand binding (Ciulli et al., 2006).

Representative data for complete biophysical characterization of inhibitor **1** are shown in Figure 2 (in Figure S3 for **2** and **3**), and results for **1–3** are summarized in Table 1. The ligands exhibited binding in all four binding assays. Binding was not detected for **4**, an analog of **1** lacking the pyrrolidine hydroxyl group (Figure S3). This is consistent with the loss of binding of nonhydroxylated relative to hydroxylated HIF-1 α peptides, supporting the hydroxyl's critical role in HIF-1 α recognition by pVHL (Hon et al., 2002). Our current best inhibitor **3** has a K_d of 5 μM , a molecular weight of 410 Da, and low lipophilicity (ClogP = -0.05), placing it in the lead-like range and resulting in good ligand efficiency and ligand lipophilicity efficiency (LE and LLE_{AT} both $0.24 \text{ kcal mol}^{-1} \text{ NHA}^{-1}$; Table 1). The latter compare very well with the average LE of $\sim 0.24 \text{ kcal mol}^{-1} \text{ NHA}^{-1}$ observed by Wells and McClendon (2007) for optimized fragments and inhibitors of a range of different PPIs. In addition, it exhibits high aqueous solubility (up to 2 mM in buffer at pH 7.0) and is Rule of 5 compliant (Table 2). Taken together, these results provided us with attractive starting points and a robust platform for a fragment deconstruction model study.

Fragmentation of Inhibitors I: Fragments Targeting a Single Subsite

With the structural and biophysical characterization of small molecule inhibitors of the pVHL:HIF-1 α interaction established, we turned to the key question of whether these compounds could have been discovered by a fragment-based approach. We first screened a small library of fragments that occupy the individual LHS, central core, and RHS subsites as part of inhibitors **1–3** (Figure 3A). Included in the library were: (1) the free carboxylate and the *i*-propylamide derivatives of the methyl-isoxazole LHS fragment (**5–6**); (2) the 4-substituted free amines and corresponding acetylated derivatives of the aromatic RHS methylbenzoate, biphenyl, and phenyl-oxazole fragments (**7–12**); and (3) the free *L*-Hyp amino acid and its neutral derivative capped on both ends, *N*-acetyl-Hyp-*N*-methyl (**13**) that bind at the central core subsite. These fragments range in size between 10 and 17 NHAs and comply with the Rule of Three (Ro3, Table 2)

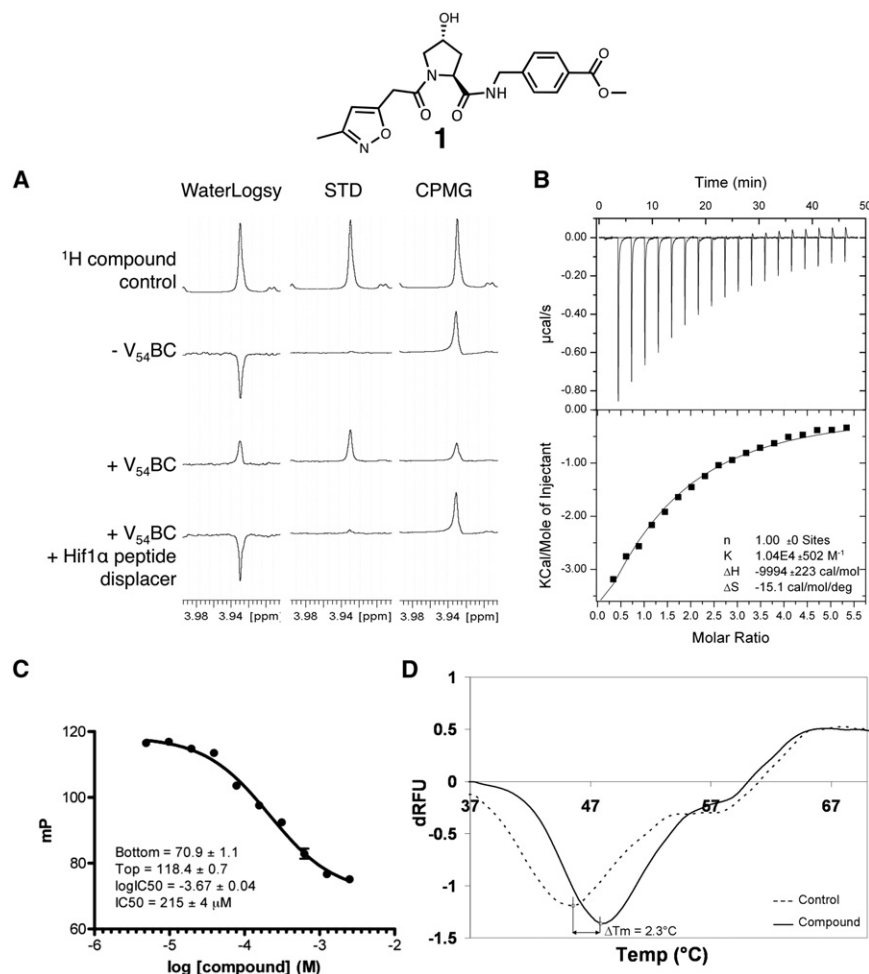


Figure 2. Biophysical Characterization of Compound 1 Binding to VCB

(A) WaterLogsy, STD, and CPMG NMR spectroscopy.

(B) Isothermal titration calorimetry.

(C) Fluorescence polarization.

(D) Differential scanning fluorimetry.

See also Figure S3.

not able to detect binding under the experimental conditions used.

Of all the fragments tested only **13** showed a very weak signal in the CPMG and WaterLOGSY NMR spectra (13% loss of CPMG signal and 1% LOGSY signal but no STD signal, Table 1). However, we could not detect any binding of **13** by DSF, FP, or competitive NMR, suggesting we would have missed this fragment if it had been present in a biophysical screen conducted under these conditions. We were also unable to detect any binding of **13** using a direct ITC experiment. On the other hand, minor perturbations of a control HIF-1 α peptide ITC titration were seen when **13** was preincubated with VCB at 5 and 10 mM concentrations (Figure S3, resulting in a back-calculated K_d of ~ 10 mM using a competitive binding model, see Supplemental Experimental Procedures). Encouraged by these results supporting binding of **13**, albeit weak, we set out to soak it at 25 mM concentration into

protein crystals and could identify clear electron density corresponding to the ligand, confirming the expected binding mode (Figure 4; Figure S1).

Fragmentation of Inhibitors II: Fragments Targeting More than One Subsite

To address the question of which size and structural complexity would be required to detect and characterize fragment binding, we expanded the promising fragment **13** toward either ends of the protein interface (Figure 3B). Larger fragments of the initial inhibitor **1** were synthesized that contained the Hyp core fragment and either a phenyl or *p*-methylbenzoate group at RHS (**14** and **16**), a methyl-isoxazole group at LHS (**15**) or both phenyl and methyl-isoxazole groups on the same compound (**17**). Fragments **14–17** exhibited NHAs ranging from 19 to 25, MW between 262 and 343 Da, ClogP < 0.2, 2 hydrogen bond donors, 3–5 hydrogen bond acceptors, and 2–4 rotatable bonds (Figure 3B; Table 2). They therefore approach the limits of, and in most cases violate, the Ro3. Evidence of binding of **14**, the only Ro3 compliant fragment, was only observed by NMR but not by DSF and FP (Table 1; Figure S3). In contrast, we were able to detect binding of the LHS-core fragment **15** and of the core-RHS fragment **16** in DSF and NMR, and to characterize their binding affinities by FP and ITC (Table 1; Figure S3). Taken

(Congreve et al., 2003), based on the ChEMBL Compound Property Definitions (<http://www.ebi.ac.uk/chemblntd/glossary>). To monitor fragment binding, we initially selected DSF, NMR spectroscopy, and FP as these techniques are widely used for first-line screening of fragment libraries (Ciulli and Abell, 2007). Fragments were tested at concentrations typically employed in these assays, that is, 5 mM for DSF, 1 mM for the three ligand-observed NMR experiments, and starting at 10 mM in 2-fold dilution dose response curves in competition with the HIF-1 α peptide for FP. Surprisingly, we were unable to unambiguously detect fragment binding directly in any of these experiments (Figure S2). In order to confirm our findings, we also assessed the ability of the fragments to displace ligand **1** in competitive NMR experiments, by monitoring the STD and WaterLOGSY signals of 0.25 mM of **1** binding to VCB in the presence and absence of 1 mM of fragments **5–13**. None of the fragments showed any evidence of competition with **1** in these experiments (data not shown). As the LHS and RHS fragments occupy nonoverlapping subsites in the inhibitors bound crystal structures, we then asked whether positive cooperativity between fragments could enhance their individual binding affinities. We therefore tested them in pairs using NMR spectroscopy and DSF to interrogate the possibility of detecting their simultaneous binding at adjacent sites (Figure S2). Again in this case, we were

Table 1. Biophysical Characterization of Small Molecules Binding to VCB

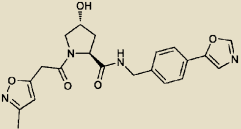
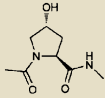
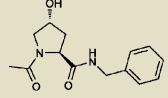
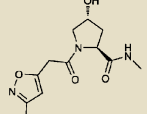
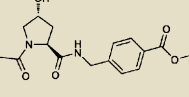
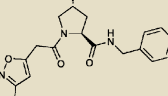
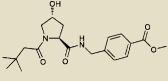
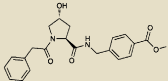
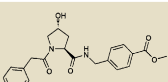
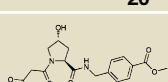
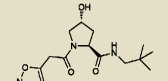
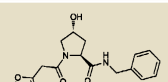
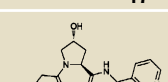
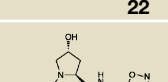
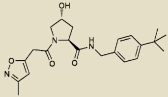
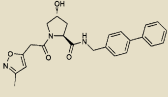
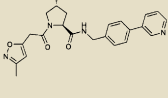
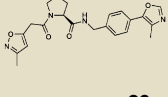
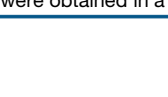
Compound	NMR Spectroscopy				DSF ΔT_m (°C)	FP K _d (μM)	ITC			LE (kcal mol ⁻¹ NHA ⁻¹)	LLE _{AT} (kcal mol ⁻¹ NHA ⁻¹)		
	Signal Monitored (ppm)	CPMG (% loss)	STD (% of 1D)	LOGSY (% of 1D)			K _d (μM)	ΔG (kcal/mol)	ΔH (kcal/mol)			-T ΔS (kcal/mol)	
 3	Isox arom	6.23	15	3.2	2.6	4.5 ± 0.0	12.5 ± 0.1	5.43 ± 0.22	-7.19 ± 0.02	-6.84 ± 0.05	0.35 ± 0.05	0.24	0.24
Hyp core  13	Acetyl	2.13	13	0	1.0	-1.4 ± 0.4	NB	K _d ≈ 10,000 ^a				0.21	0.40
 14	Acetyl	2.13	45	2.0	3.1	0.2 ± 0.0	NB	ND				ND	ND
RHS1 Ref  15	Isox arom	6.27	53	4.5	8.0	2.1 ± 0.4	660 ± 15	242 ^a	-4.94 ^a	-5.76 ^a	0.82 ^a	0.24	0.36
LHS Ref  16	OMe	3.94	26	3.2	2.1	1.7 ± 0.4	150 ± 2	270 ± 4	-4.88 ± 0.01	-4.35 ± 0.02	-0.53 ± 0.02	0.21	0.21
RHS2 Ref  17	Isox arom	6.26	36	3.6	1.5	1.4 ± 0.0	295 ± 3	600 ± 17	-4.40 ± 0.02	-12.20 ± 0.20	7.80 ± 0.20	0.18	0.17

Table 1. Continued

Compound	NMR Spectroscopy				DSF	FP	ITC			LE (kcal mol ⁻¹ NHA ⁻¹)	LLE _{AT} (kcal mol ⁻¹ NHA ⁻¹)		
	Signal Monitored (ppm)	CPMG (% loss)	STD (% of 1D)	LOGSY (% of 1D)			ΔT _m (°C)	K _d (μM)	K _d (μM)			ΔG (kcal/mol)	ΔH (kcal/mol)
LHS  18	OMe	3.93	39	9.2	5.4	4.5 ± 0.7	53.2 ± 0.7	45.5 ± 2.6	-5.93 ± 0.04	-3.42 ± 0.12	-2.51 ± 0.12	0.21	0.12
 19	OMe	3.94	70	11.1	2.1	-0.5 ± 0.3	165 ± 7	280 ± 10	-4.85 ± 0.02	-1.89 ± 0.04	-2.96 ± 0.04	0.17	0.08
 20	OMe	3.93	55	9.3	0	0.5 ± 0.0	580 ± 14	665 ^a	-4.34 ^a	-5.90 ^a	1.55 ^a	0.15	0.13
 1	OMe	3.93	29	9.4	5.5	2.3 ± 0.0	86.1 ± 1.6	96.2 ± 4.6	-5.48 ± 0.03	-9.99 ± 0.22	4.51 ± 0.22	0.19	0.18
RHS1  21	Isox arom	6.27	19	1.1	2.0	-0.2 ± 0.3	1,106 ± 21	ND				0.17	0.16
 17	Isox arom	6.26	36	3.6	1.5	1.4 ± 0.0	295 ± 3	600 ± 17	-4.40 ± 0.02	-12.20 ± 0.20	7.80 ± 0.20	0.18	0.17
 22	Isox arom	6.24	18	1.2	5.1	0.5 ± 0.0	452 ± 6	435 ± 8	-4.59 ± 0.01	-8.65 ± 0.09	4.06 ± 0.08	0.18	0.25
 23	Isox arom	6.26	57	2.6	6.9	0.9 ± 0.0	343 ± 4	350 ± 17	-4.72 ± 0.03	-8.13 ± 0.22	3.41 ± 0.02	0.19	0.27

(Continued on next page)

Table 1. Continued

Compound	NMR Spectroscopy					DSF ΔT_m (°C)	FP K _d (μM)	ITC K _d (μM)	ΔG (kcal/mol)	ΔH (kcal/mol)	- ΔS (kcal/mol)	LE	LLE _{AT}	
	Signal Monitored (ppm)	CPMG (% loss)	STD (% of 1D)	LOGSY (% of 1D)	(kcal mol ⁻¹ NHA ⁻¹)							(kcal mol ⁻¹ NHA ⁻¹)		
RHS2		Isox arom	6.26	55	3.4	4.1	1.4 ± 0.0	821 ± 12	ND			0.14	0.05	
24		Isox arom	6.26	70	19	19	5.5 ± 0.0	27.7 ± 0.2	ND			0.20	0.11	
2		Isox arom	6.24	28	3.5	4.7	3.2 ± 0.0	20.3 ± 0.5	14.9 ± 0.8	-6.59 ± 0.03	-4.84 ± 0.06	-1.75 ± 0.06	0.21	0.18
25		Isox arom	6.23	15	1.3	5.1	6.8 ± 0.0	3.6 ± 0.1	7.35 ± 0.36	-7.01 ± 0.03	-5.62 ± 0.05	-1.39 ± 0.06	0.23	0.23
26														

ND, not determined; NB, no binding. See also [Figure S4](#) and [Table S2](#).

^aThese data were obtained in a competitive ITC assay.

Table 2. Physicochemical Properties of Inhibitors 1–3 and Fragments 5–17

Inhibitors													
Properties (Ro5)	1			2			3						
MW (≤ 500 Da)	401			419			410						
cLogP (≤ 5)	0.14			2.06			−0.05						
HBD (≤ 5)	2			2			2						
HBA (≤ 10)	7			5			7						
Rot. bonds (≤ 5)	5			5			5						
Ro5 compliant	✓			✓			✓						
NMR	✓			✓			✓						
DSF	✓			✓			✓						
ITC	✓			✓			✓						
FP	✓			✓			✓						
Fragments													
Properties (Ro3)	13	5	6	7	8	9	10	11	12	14	15	16	17
NHA	13	13	10	12	15	14	17	13	16	19	19	23	25
MW (≤ 300 Da)	186	182	141	165	207	183	225	174	216	262	267	320	343
cLogP (≤ 3)	−1.84	−0.22	−0.34	1.06	0.92	2.98	2.84	0.87	0.73	0.04	−1.71	0.01	0.17
HBD (≤ 3)	2	1	1	1	1	1	1	1	1	2	2	2	2
HBA (≤ 3)	3	2	3	2	2	1	1	1	2	3	5	5	5
Rot. bonds (≤ 3)	0 ^a	3	2	2 ^b	3 ^b	2	3	2	3	2 ^a	2 ^a	4 ^a	4 ^a
PSA (≤ 60)	69.6	50.7	64.7	52.3	55.4	26.0	29.1	47.6	50.7	69.6	91.2	95.9	91.2
Ro3 compliant	✓ ^c	✓	✓ ^c	✓	✓	✓	✓	✓	✓	✓ ^c	✗	✗	✗
NMR	✗	✗	✗	✗	✗	✗	✗	✗	✗	✓	✓	✓	✓
DSF	✗	✗	✗	✗	✗	✗	✗	✗	✗	✗	✓	✓	✓
FP	✗	✗	✗	✗	✗	✗	✗	✗	✗	✗	✓	✓	✓
ITC	✗	-	-	-	-	-	-	-	-	-	✓	✓	✓

✓, yes or true; ✗, not or false.

^aThe C(α)–C(O) bond of the Hyp core, about which rotation is described by the Ramachandran ψ dihedral angle, was not counted as a rotatable bond.

^bThe C(O)–O bond of the methyl ester was not counted as a rotatable bond.

^cNot considering the requirement for PSA.

together, these results point to the requirement of fragments of the starting inhibitors to form favorable interactions in at least two subsites of the pVHL–HIF-1 α interface. This was confirmed by the ability to detect and fully characterize the binding of two dipeptides derived from HIF-1 α , Ala–Hyp, and Hyp–Tyr (Figure S2). Compound **17**, spanning the three subsites LHS–Hyp–RHS, also yielded binding data across the full spectrum of biophysical techniques.

Fragmentation of Inhibitors III: Deconstructing Ligand and Group Efficiencies

With the first two questions addressed, we asked whether we could identify preferential “hot spots” for fragment binding at the protein interface. The lack of quantitative binding for the smaller fragments **5–13** meant that an indirect approach was needed to tackle this problem. As binding of **15**, **16**, and **17** could be reliably characterized biophysically, these were chosen as reference compounds to anchor fragments covalently in order to study their contributions to binding at three distinct subsites, LHS, RHS1, and RHS2 (Figure 3). We thus designed a library of 12 compounds (**1**, **2**, and **17–26**) each containing a small probe fragment, either *t*-butyl, phenyl, pyridyl, or Me-(is)oxazole, attached to the appropriate side of each reference compound (Figure 3C). These groups were

chosen as they had (1) similar size (4–6 NHAs) and would be sufficiently small to fit in each subsite of the interface; (2) different values of CLogP ranging from 0.6 to 3.1; and (3) different shapes. Binding of compounds **17–26** was fully characterized by all four biophysical techniques (see Figure S3 and results summarized in Table 1). A good correlation was seen between the K_d values measured directly by ITC and those back calculated from the IC₅₀ values measured by FP (Table 1; Figure S4), justifying their use in cases in which ITC data could not be obtained (in other cases the average K_d value was used to calculate ΔG s).

In order to quantify and dissect the contributions of each group at each individual subsite, we measured their group efficiency (GE), defined as binding energy per heavy atom of a group of the molecule

$$GE = \frac{-\Delta\Delta G}{\Delta NHA}$$

GE scales affinity by size in a fashion consistent with ligand efficiency, with a value of 0.3 kcal mol^{−1} NHA^{−1} usually taken as a reference threshold (Congreve et al., 2008). To take into account not only size but also lipophilicity, we also calculated ligand lipophilicity efficiency (LLE_{AT}) and group lipophilicity efficiency (Mortenson and Murray, 2011)

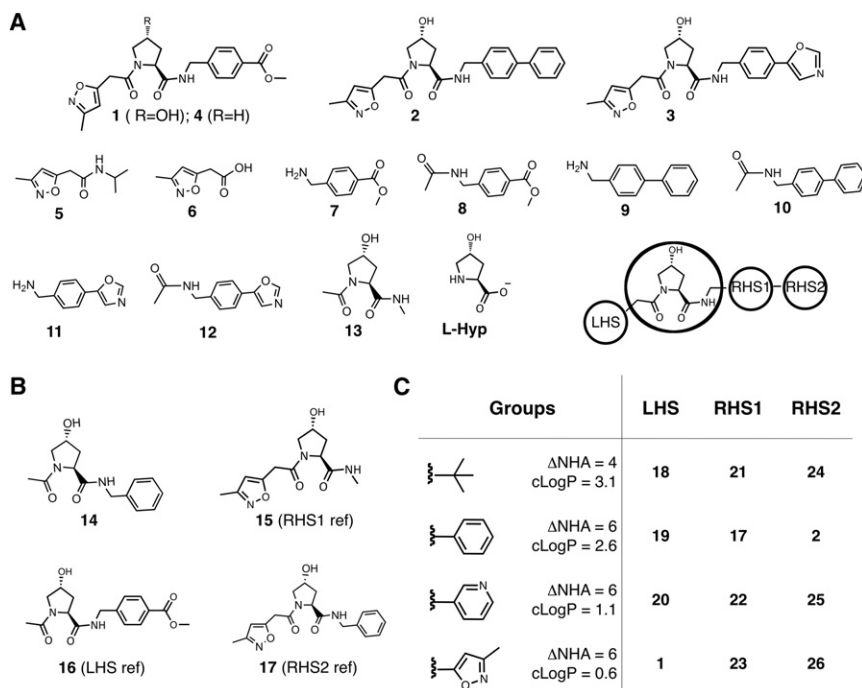


Figure 3. Small Molecule Library Used to Probe the pVHL:HIF-1 α Interaction

(A) Micromolar small molecule inhibitors **1–3** used for the biophysical and structural characterization of the pVHL:ligand interactions and fragments used to probe individual subsites.

(B) Fragments designed to probe more than one subsite, including reference molecules used to calculate group efficiencies and group lipophilicity efficiencies.

(C) Library of compounds placing a *t*-butyl, phenyl, pyridyl, or Me-(is)oxazole group at the left-hand site (LHS), right-hand site 1 (RHS1), or 2 (RHS2). ClogP values are not defined for groups and depend on the context of the whole molecule. The values listed were calculated for parent molecules containing a methyl attached to each group. See also Figure S2.

10 mM as determined by competitive ITC. To bring the contributions of **13** as a group onto the same scale as the corresponding terms for other groups, the rigid-body barrier to binding, estimated to be +4.2 kcal/mol (Murray and Verdonk, 2002), was subtracted from the free

energy of binding of **13** as previously described (Saxty et al., 2007). Although this value is widely used, it can vary depending on the types of interactions formed. Indeed, others have reported values in the range of 6–12 kcal/mol for this term (Page and Jencks, 1971; Lundquist and Toone, 2002); hence, we may be underestimating the magnitude of the correction due to the entropic barrier. This analysis yielded the largest group-based values for **13** (GE = 0.53, $\text{GLE}_{\text{AT}} = 0.72$), reinforcing its role as a good anchoring fragment and defining the core subsite as the hot spot that contains the bulk of the binding energy. Group efficiencies calculated for the LHS isoxazole (GE = 0.08) and the RHS methylbenzoate (0.09), biphenyl (0.14), and phenyl-oxazole (0.21) correspond to $\Delta\Delta\text{G}$ s of -0.9 , -1.6 , and -2.3 kcal/mol, respectively. These values are all much smaller than the rigid-body barrier to binding, therefore allowing a retrospective rationalization of why the starting LHS and RHS fragments **5–12** did not bind.

To analyze all the group contributions, we clustered GEs within each subsite, allowing comparison of how each individual subsite interacts with different fragments (Figure 5B, top). In addition, we clustered GLE_{AT} s by the individual group, highlighting how each group probes the different subsites (Figure 5B, bottom). The LHS subsite responded favorably to the binding of the methyl-isoxazole group. The largest GE value, however, was seen for the *t*-butyl group. This is in marked contrast to RHS1 and RHS2 that were more discriminating against this group, highlighting the promiscuous nature of the solvent-exposed LHS subsite. RHS2 appears to be a second hot spot for fragment binding, as it exhibited the highest average GE value across the group series (0.15). Importantly, all groups, except *t*-butyl, had their highest GE and GLE_{AT} at this subsite. This may be due to a more pocket-like shape of RHS2, whereas the observed flexibility of the R107 side chain may allow larger groups to be

$$\text{GLE}_{\text{AT}} = 0.19 + RT \ln(10) \frac{\Delta pK_d - \Delta \text{cLogP}}{\Delta \text{NHA}}$$

For consistency, both metrics have been designed to have the same reference value of $0.3 \text{ kcal mol}^{-1} \text{ NHA}^{-1}$ as LE and GE, respectively, hence providing meaningful comparisons between them.

Compounds exhibited LE values ranging from 0.14 to 0.24 (Table 1, average LE = $0.19 \pm 0.03 \text{ kcal mol}^{-1} \text{ NHA}^{-1}$). Taking lipophilicity into account, the differences between the ligands become more pronounced, with LLE_{AT} ranging from as little as 0.05 for **24** up to 0.36 for **15** (Table 1, average LLE_{AT} = $0.19 \pm 0.09 \text{ kcal mol}^{-1} \text{ NHA}^{-1}$), reflecting the wide range of lipophilicities introduced by the chosen groups. Despite the challenges we faced at detecting and measuring binding of the capped Hyp **13**, its small size (NHA = 13) and hydrophilic nature (ClogP = -1.8) result in the highest LLE_{AT} (0.40) across the series based on an estimated K_d of 10 mM from competition ITC experiments. The group-based parameters are on average much lower in value than the corresponding ligand-based parameters, indicating that the groups are not able to maintain the level of ligand efficiencies observed with **3** and reference compounds **15–17**. However, group efficiencies are spread over a wider range (Figure 5A, average GE = 0.07 ± 0.23 and average GLE_{AT} = -0.13 ± 0.43) and hence provide a more informative set of parameters to monitor than ligand based efficiencies to probe the individual subsites.

Dissecting Hot Spots of Fragments Targeting Individual Subsites

As binding could not be measured for any fragment lacking the central Hyp core, we can only estimate the group efficiencies of **13** based on a ΔG of -2.8 kcal/mol associated to its K_d of

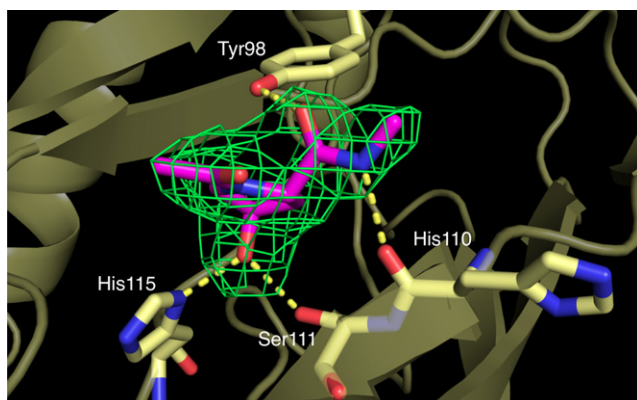


Figure 4. X-Ray Crystal Structure of Fragment 13 Bound to VCB, Solved at 2.50 Å of Resolution

Fragment **13** is shown in stick representation (magenta carbons), whereas pVHL is shown in light yellow cartoon representation. Key amino acids interacting with the fragment are shown in sticks, with carbon atoms in the same color. The $F_o - F_c$ omit electron density map associated with the fragment is shown as a green mesh contoured at 3σ . See also Figure S1.

accommodated favorably. It is interesting to note that the natural substrate HIF-1 α does not fully explore the binding potential of this subsite as Ile566, despite being important for binding (Min et al., 2002), is only partly buried in this pocket (Figure 1B). In contrast to RHS2, RHS1 yielded negative, unfavorable GE values for all groups tested, and the lowest average GE (-0.11), suggesting it is the least “druggable” subsite. The poor GE of the phenyl group is consistent with the weak binding shown by fragment **14**. It is possible that the best group is not among those tested or that they are not accommodated for in their optimal position due to conformational restriction provided by the methylene group linking RHS1 groups to the amide bond of Hyp. Our results suggest that RHS1 could be a good place to concentrate future medicinal chemistry optimization to improve the current ligands, also given its role as a linker region between the two identified hot spots, the core and RHS2 subsites.

DISCUSSION

Despite its rather modest affinity of ~ 10 mM, the hydroxyproline di-amide **13** contributes the most to the initial inhibitor binding free energy. This becomes evident once this and the overall ligand efficiency are corrected for the entropic rigid body barrier to binding. Yet, this fragment could not be readily detected by techniques routinely used for fragment screening. Similarly, binding was not detected for any fragments targeting the LHS or RHS pockets on pVHL, individually or in combinations. These results were unanticipated because (1) it is often observed that fragments have higher ligand efficiency than the larger compounds they are part of, and (2) we would have expected to detect binding of some of the fragments even if they had only retained the ligand efficiency of the parent inhibitors (Table S2). They also contrast with the results of a previous study in which the binding of 19/22 fragments of nine known PPI inhibitors of Bcl-x $_L$ was detected (Barelier et al., 2010). However, in that case, the initial inhibitors were much larger than in our study and included some that were discovered using FBLD, so detec-

A

GE & GLE (kcal mol ⁻¹ NHA ⁻¹)	LHS	Hyp core	RHS 1	RHS 2
	0.21 -0.41		-0.24 -0.75	-0.20 -0.70
	0.00 -0.43	0.53 0.72	-0.07 -0.42	0.20 -0.15
	-0.11 -0.19		-0.07 -0.08	0.24 0.23
	0.08 0.05		-0.05 0.00	0.35 0.48

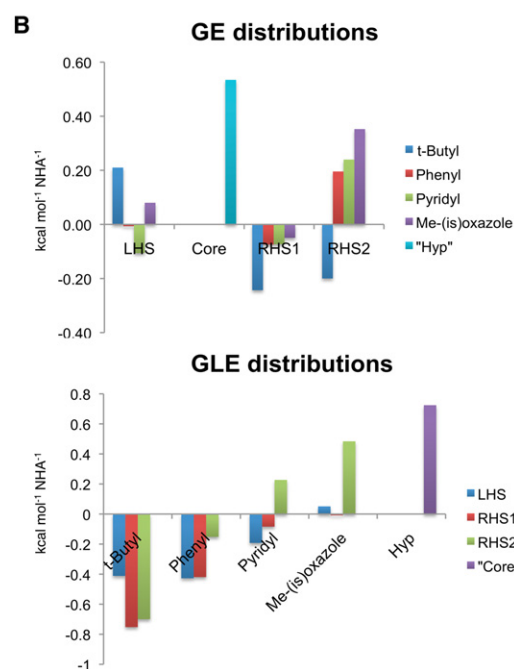


Figure 5. Group Efficiencies and Group Lipophilic Efficiencies of Small Molecules Binding to VCB

Values for GE (black) and GLE_{AT} (red) for each group at the different positions (LHS, RHS1, and RHS2) are listed in (A), and their distributions, according to position or group, respectively, are shown in (B).

tion of fragment binding was perhaps not surprising. Our results point to the possibility that current fragment screens against PPIs may be missing interesting fragments because of the inherently low ligand efficiencies associated with binding small molecules at protein surfaces. The pVHL:HIF-1 α interaction recapitulates many of the features of PPIs that appear to be important in determining such low ligand efficiencies: (1) the displacement of bound water molecules, as required with binding of the Hyp core; (2) the exploration of cryptic pockets at the protein surface, as in the case of the RHS2 pocket opening upon conformational change of R107; and (3) the interaction with subsites that the natural protein partner does not engage with or does suboptimally, as in the case of Ile566 of HIF-1 α . These features would all contribute to low affinities of small, unanchored fragments, preventing their detection in screens

in most cases. Our study nevertheless suggests that even much weaker and less ligand efficient fragments ($K_d \approx 10$ mM, $LE \sim 0.2$ kcal mol⁻¹ NHA⁻¹ as for the Hyp fragment **13**) than those typically found at enzyme active sites (K_d 0.1–1.0 mM, $LE > 0.3$ kcal mol⁻¹ NHA⁻¹), would still be useful starting points in the construction of promising small molecules, as they can generate much more interaction energy with the protein than their modest affinities would lead one to suppose. This underscores the challenge of reliably detecting such weak but highly specific interactions in screens while at the same time discriminating against nonspecific binding or artifactual effects. It further highlights the importance of employing a range of orthogonal screening strategies of sufficiently sensitive biophysical techniques to allow robust identification of weak binders as hits and their subsequent characterization and validation.

As fragments became more complex and began targeting at least two subsites at the pVHL:HIF-1 α interface rather than a single one, we could unambiguously detect and characterize their binding. Fragments **15** and **16** explore a higher level of molecular complexity than the initial fragments **5–13**, violate the Ro3, and would have likely failed to pass filters commonly applied to construct current fragment libraries. To this end, a recent study has suggested that alleviating some of these strict criteria can lead to higher hit rates of fragments and still identify suitable starting points for future design (Köster et al., 2011). Both **15** and **16** contain an aromatic ring attached to an amino acid moiety. Similarly, we were able to measure binding of the corresponding di-amino acid fragments. These observations tempt us to speculate that aromatic/amino acid or di-amino acid fragments that approach or break the limits of the Ro3 could be privileged scaffolds against PPIs. Their inclusion in focused fragment libraries aimed at targeting PPIs could lead to increased hit rates from screens and could facilitate the identification of novel binding sites. To this end, screens of a $\sim 1,300$ commercially available Ro3-compliant fragment library have to date proved unsuccessful in our experience against this PPI. Taken together, our results suggest that the tractability of PPIs may be a more complex feature than can be simply assessed by screening of Ro3-compliant fragment libraries and point to the need of sampling more complex chemical space.

In addition to asking whether fragments of initial ligands can be detected, one can ask whether ligands can always be parsed into fragments that maintain the observed binding mode. This question has been addressed for enzyme substrates and coenzymes (Stout et al., 1998; Ciulli et al., 2006), enzyme inhibitors (Babaoglu and Shoichet, 2006; Nazaré et al., 2012), and PPI inhibitors (Barelier et al., 2010). It has been observed that smaller fragments do not always recapitulate their binding mode as part of the initial ligands. However, sufficiently elaborate fragments often do so (Babaoglu and Shoichet, 2006; Barelier et al., 2010). The results of our study are consistent with this observation, as binding of fragments could be detected only as they became larger. As the Hyp core fragment **13** retains the binding mode, it is reasonable to expect that the larger fragments **15–17** also do so.

To evaluate the contributions of the smaller fragments to the binding free energy and to further rationalize our inability to detect their binding, we anchored them around the Hyp core and modularly deconstructed their ligand and group lipophilicity

efficiencies. To our knowledge, this study reports the first example of using GE and GLE_{AT} together to probe interactions of fragments at distinct subsites of a PPI. In addition, this approach can guide the design of PPI ligands while preventing them from becoming too large and lipophilic. Optimization programs that solely make use of LE or GE metrics as guidelines would favor hydrophobic binders bearing undesired physicochemical properties. On the other hand, LLE_{AT} and GLE_{AT} would favor hydrophilic binders that may not pass biological barriers. The combination of both metrics is therefore proposed as a balanced guide to compound optimization and is being used to develop improved inhibitors of the pVHL:HIF-1 α interaction.

In summary, we report, to our knowledge, the first, comprehensive deconstructive study of known inhibitors of a protein-protein interaction into fragments. Our group analysis, based on thorough biophysical and structural characterization, demonstrates how a fragment-based approach can be used to dissect binding hot spots, analyze their key features, and rationalize fragment contributions at protein-protein interfaces. We therefore provide a general methodology that can be applied to characterize other protein-protein interactions and their small molecule binders. Perhaps more importantly, the observations emerged from our study of the pVHL:HIF-1 α interaction could prove useful in addressing the challenges faced when interrogating the ligandability of other difficult PPI targets by fragment-based approaches.

SIGNIFICANCE

We have presented a deconstructive study of fragments of a protein-protein interface (PPI) inhibitor. Over the past 15 years, fragment-based lead discovery (FBLD) has established itself as a powerful approach to develop small molecule binders of desired potency and physicochemical properties. It is anticipated that FBLD may address the well-documented failures of, for example, high-throughput screening against more challenging targets, such as PPIs (Murray et al., 2012). However, the potential and limitations of biophysical fragment screening to assess the tractability of PPIs have been underexplored. Our findings point to the possibility that screening Rule of Three compliant libraries may result in missing highly group-efficient and useful fragments, as they could bind too weakly to be detected. We therefore propose that the most fruitful fragments to screen against PPIs should be somewhat larger than those commonly used for more druggable targets and could include “privileged” structures, such as aromatic-amino acid hybrid compounds.

The model system investigated, that is, the interaction between the von Hippel Lindau protein (pVHL) and the alpha subunit of hypoxia-inducible factor 1 (HIF-1 α), involves recognition of a flexible peptide lacking secondary structure and of a posttranslational modification. There is increasing evidence that these features render a PPI more ligandable than, for example, obligate PPIs involving large and flat interfaces (Surade and Blundell, 2012), and that these types of PPIs are providing new therapeutic opportunities (Filippakopoulos et al., 2010). Given its many important biological roles as a tumor suppressor protein and as an E3 ligase in

oxygen sensing, pVHL is per se an attractive target for the development of small molecule therapeutics and probes. The methodology reported here, integrating GE and GLE analyses to dissect fragment binding, will guide the optimization of future pVHL ligands and can be applied to probe hot spots at other PPIs.

EXPERIMENTAL PROCEDURES

VCB and VCBH Cloning, Expression, Purification, and Crystallization

The pVHL:ElonginC:ElonginB (VCB) complex was expressed, purified, and crystallized as previously described (Buckley et al., 2012). In order to purify the complex between VCB and a 19-mer HIF-1 α peptide (DEALAHypYIP MDDDFQLRSF) (VCBH), VCB was mixed with a 2-fold excess of the peptide. The excess of peptide was subsequently removed using a Superdex75 10/300 GL column, equilibrated in 20 mM Bis-Tris (pH 7.0), 150 mM NaCl, and 1 mM DTT. VCBH was crystallized in 0.1 M K phosphate (pH 6.6), 0.2 M (NH₄)₂SO₄, 20% PEG MME 5000, and 5 mM DTT, at 296 K, using hanging drop vapor diffusion.

X-Ray Diffraction, Data Collection, and Crystal Structures Solution

X-ray data collection, structure solution, and refinement parameters for VCB-3 liganded structure were described previously (Buckley et al., 2012). Details of the data collection and structure determination of VCB-1, VCB-2, VCB-13, and VCBH structures can be found in Supplemental Experimental Procedures.

Differential Scanning Fluorimetry

DSF experiments (Kranz and Schalk-Hihi, 2011) were performed using a Roche Lightcycler 480 machine, in a 96-well plate setup, using 100 μ l per well. Compounds were assayed at 1 mM concentration (or 5 mM for fragments targeting one subsite) in triplicates, using a concentration of 5 μ M VCB in 100 mM Tris (pH 8.5), 100 mM NaCl, 2.5 \times Sypro Orange, and 5% v/v DMSO. Data were recorded during a continuous scan from 37°C to 95°C. The fluorescence excitation and emission wavelengths were 483 and 533 nm.

NMR Spectroscopy

¹H NMR spectroscopic experiments were performed at 278 K on a 700 MHz Bruker NMR spectrometer equipped with a 5 mm triple TXI cryoprobe with z gradients. The resulting spectra were analyzed using the Bruker TopSpin software. For direct binding experiments, each compound was run as three samples, made up to 200 μ l in 3 mm capillaries, according to the following compositions (Trimethylsilyl-propionic acid-*d*₄ [TSP] was present in all samples for calibration purposes): (1) Control sample = 1 mM compound, 2% (v/v) *d*₆-DMSO, 20 μ M TSP, 50 mM NaPO₄ (pH 7.0), and 10% (v/v) D₂O; (2) + protein sample = control sample + 10 μ M VCB complex; (3) + protein + displacer sample = control sample + 10 μ M VCB complex + 500 μ M HIF-1 α 10-mer peptide (DEALAHypYIPD). For competition binding experiments, each sample contained 0.25 mM of **1**, 10 μ M protein in the same buffer conditions as above, and in the absence or presence of 1 mM fragments **5–13**. More detailed information on the pulse sequences used in the WaterLOGSY, STD, and CPMG experiments can be found in Supplemental Experimental Procedures.

Fluorescence Polarization

Fluorescence polarization measurements were recorded on a BMG LABTECH PHERAstar Plus instrument as described in Supplemental Experimental Procedures. The fluorescence excitation and emission wavelengths were 485 and 520 nm. Data were fitted using GraphPad Prism 5. *K_d* values for the compound-VCB interaction were back-calculated from the measured IC₅₀ values as described in Supplemental Experimental Procedures.

Isothermal Titration Calorimetry

ITC experiments were performed on an ITC₂₀₀ instrument from Microcal Inc. (GE Healthcare, Waukesha, WI, USA) at 25°C as described in Supplemental Experimental Procedures.

Synthetic Procedures

Detailed information on synthetic procedures is in Supplemental Experimental Procedures.

ACCESSION NUMBERS

The atomic coordinates and structure factors of the *Homo sapiens* pVHL_{54–213}:ElonginC:ElonginB in complex with **1** (2.79 Å), **2** (2.65 Å), **3** (2.90 Å), and **13** (2.5 Å) and the HIF-1 α peptide DEALAHypYIPMDDDFQLRSF (1.73 Å) have been deposited in the Protein Data Bank (PDB) with accession codes 3ztd, 3ztc, 3zrc, 4awj, and 4ajy, respectively.

SUPPLEMENTAL INFORMATION

Supplemental Information includes two tables, four figures, and Supplemental Experimental Procedures and can be found with this article online at <http://dx.doi.org/10.1016/j.chembiol.2012.08.015>.

ACKNOWLEDGMENTS

This work was funded in part by the U.K. Biotechnology and Biological Sciences Research Council (grant no. BB/G023123/1) (BBSRC David Phillips Fellowship to A.C.), the EC PIEF-GA-2010-275683 (Marie-Curie Intra European Fellowship to I.V.M.), and the U.S. National Institutes of Health (NIH AI084140 to C.M.C.). We thank Beau Schofield for the synthesis of fragment **10**. We are grateful to Dr. Dimitri Y. Chirgadze of the Crystallographic X-Ray Facility at the Department of Biochemistry, University of Cambridge and to the technical support at the ESRF, Soleil and Diamond Synchrotron Facilities, for their assistance.

Received: June 8, 2012

Revised: August 10, 2012

Accepted: August 16, 2012

Published: October 25, 2012

REFERENCES

- Babaoglu, K., and Shoichet, B.K. (2006). Deconstructing fragment-based inhibitor discovery. *Nat. Chem. Biol.* **2**, 720–723.
- Barelief, S., Pons, J., Marcillat, O., Lancelin, J.-M., and Krimm, I. (2010). Fragment-based deconstruction of Bcl-x_L inhibitors. *J. Med. Chem.* **53**, 2577–2588.
- Basse, N., Kaar, J.L., Settanni, G., Joerger, A.C., Rutherford, T.J., and Fersht, A.R. (2010). Toward the rational design of p53-stabilizing drugs: probing the surface of the oncogenic Y220C mutant. *Chem. Biol.* **17**, 46–56.
- Braisted, A.C., Oslob, J.D., Delano, W.L., Hyde, J., McDowell, R.S., Waal, N., Yu, C., Arkin, M.R., and Raimundo, B.C. (2003). Discovery of a potent small molecule IL-2 inhibitor through fragment assembly. *J. Am. Chem. Soc.* **125**, 3714–3715.
- Buckley, D.L., Van Molle, I., Gareiss, P.C., Tae, H.S., Michel, J., Noblin, D.J., Jorgensen, W.L., Ciulli, A., and Crews, C.M. (2012). Targeting the von Hippel-Lindau E3 ubiquitin ligase using small molecules to disrupt the VHL/HIF-1 α interaction. *J. Am. Chem. Soc.* **134**, 4465–4468.
- Ciulli, A., and Abell, C. (2007). Fragment-based approaches to enzyme inhibition. *Curr. Opin. Biotechnol.* **18**, 489–496.
- Ciulli, A., Williams, G., Smith, A.G., Blundell, T.L., and Abell, C. (2006). Probing hot spots at protein-ligand binding sites: a fragment-based approach using biophysical methods. *J. Med. Chem.* **49**, 4992–5000.
- Congreve, M., Carr, R., Murray, C., and Jhoti, H. (2003). A 'rule of three' for fragment-based lead discovery? *Drug Discov. Today* **8**, 876–877.
- Congreve, M., Chessari, G., Tisi, D., and Woodhead, A.J. (2008). Recent developments in fragment-based drug discovery. *J. Med. Chem.* **51**, 3661–3680.
- Coyne, A.G., Scott, D.E., and Abell, C. (2010). Drugging challenging targets using fragment-based approaches. *Curr. Opin. Chem. Biol.* **14**, 299–307.

- Crews, C.M. (2010). Targeting the undruggable proteome: the small molecules of my dreams. *Chem. Biol.* **17**, 551–555.
- Dalvit, C., Fogliatto, G., Stewart, A., Veronesi, M., and Stockman, B. (2001). WaterLOGSY as a method for primary NMR screening: practical aspects and range of applicability. *J. Biomol. NMR* **21**, 349–359.
- Edfeldt, F.N.B., Folmer, R.H.A., and Breeze, A.L. (2011). Fragment screening to predict druggability (ligandability) and lead discovery success. *Drug Discov. Today* **16**, 284–287.
- Erlanson, D.A., Braisted, A.C., Raphael, D.R., Randal, M., Stroud, R.M., Gordon, E.M., and Wells, J.A. (2000). Site-directed ligand discovery. *Proc. Natl. Acad. Sci. USA* **97**, 9367–9372.
- Erlanson, D.A., McDowell, R.S., and O'Brien, T. (2004). Fragment-based drug discovery. *J. Med. Chem.* **47**, 3463–3482.
- Fauman, E.B., Rai, B.K., and Huang, E.S. (2011). Structure-based druggability assessment—identifying suitable targets for small molecule therapeutics. *Curr. Opin. Chem. Biol.* **15**, 463–468.
- Filippakopoulos, P., Qi, J., Picaud, S., Shen, Y., Smith, W.B., Fedorov, O., Morse, E.M., Keates, T., Hickman, T.T., Felletar, I., et al. (2010). Selective inhibition of BET bromodomains. *Nature* **468**, 1067–1073.
- Hajduk, P.J., and Greer, J. (2007). A decade of fragment-based drug design: strategic advances and lessons learned. *Nat. Rev. Drug Discov.* **6**, 211–219.
- Hajduk, P.J., Huth, J.R., and Fesik, S.W. (2005). Druggability indices for protein targets derived from NMR-based screening data. *J. Med. Chem.* **48**, 2518–2525.
- Hajduk, P.J., Galloway, W.R.J.D., and Spring, D.R. (2011). Drug discovery: A question of library design. *Nature* **470**, 42–43.
- Higuero, A.P., Schreyer, A., Bickerton, G.R.J., Pitt, W.R., Groom, C.R., and Blundell, T.L. (2009). Atomic interactions and profile of small molecules disrupting protein-protein interfaces: the TIMBAL database. *Chem. Biol. Drug Des.* **74**, 457–467.
- Hon, W.-C., Wilson, M.I., Harlos, K., Claridge, T.D.W., Schofield, C.J., Pugh, C.W., Maxwell, P.H., Ratcliffe, P.J., Stuart, D.I., and Jones, E.Y. (2002). Structural basis for the recognition of hydroxyproline in HIF-1 alpha by pVHL. *Nature* **417**, 975–978.
- Hopkins, A.L., Groom, C.R., and Alex, A. (2004). Ligand efficiency: a useful metric for lead selection. *Drug Discov. Today* **9**, 430–431.
- Jaakkola, P., Mole, D.R., Tian, Y.M., Wilson, M.I., Gielbert, J., Gaskell, S.J., Kriegsheim, A.v., Hebestreit, H.F., Mukherji, M., Schofield, C.J., et al. (2001). Targeting of HIF-alpha to the von Hippel-Lindau ubiquitylation complex by O₂-regulated prolyl hydroxylation. *Science* **292**, 468–472.
- Kaelin, W.G., Jr. (2008). The von Hippel-Lindau tumour suppressor protein: O₂ sensing and cancer. *Nat. Rev. Cancer* **8**, 865–873.
- Kozakov, D., Hall, D.R., Chuang, G.-Y., Cencic, R., Brenke, R., Grove, L.E., Beglov, D., Pelletier, J., Whitty, A., and Vajda, S. (2011). Structural conservation of druggable hot spots in protein-protein interfaces. *Proc. Natl. Acad. Sci. USA* **108**, 13528–13533.
- Köster, H., Craan, T., Brass, S., Herhaus, C., Zentgraf, M., Neumann, L., Heine, A., and Klebe, G. (2011). A small nonrule of 3 compatible fragment library provides high hit rate of endothiapepsin crystal structures with various fragment chemotypes. *J. Med. Chem.* **54**, 7784–7796.
- Kranz, J.K., and Schalk-Hihi, C. (2011). Protein thermal shifts to identify low molecular weight fragments. *Methods Enzymol.* **493**, 277–298.
- Larsson, A., Jansson, A., Åberg, A., and Nordlund, P. (2011). Efficiency of hit generation and structural characterization in fragment-based ligand discovery. *Curr. Opin. Chem. Biol.* **15**, 482–488.
- Leeson, P.D., and Springthorpe, B. (2007). The influence of drug-like concepts on decision-making in medicinal chemistry. *Nat. Rev. Drug Discov.* **6**, 881–890.
- Loenarz, C., Mecinović, J., Chowdhury, R., McNeill, L.A., Flashman, E., and Schofield, C.J. (2009). Evidence for a stereoelectronic effect in human oxygen sensing. *Angew. Chem. Int. Edit. Engl.* **48**, 1784–1787.
- Lundquist, J.J., and Toone, E.J. (2002). The cluster glycoside effect. *Chem. Rev.* **102**, 555–578.
- Mayer, M., and Meyer, B. (1999). Characterization of ligand binding by saturation transfer difference NMR spectroscopy. *Angew. Chem. Int. Edit. Engl.* **38**, 1784–1788.
- Maurer, T., Garrenton, L.S., Oh, A., Pitts, K., Anderson, D.J., Skelton, N.J., Fauber, B.P., Pan, B., Malek, S., Stokoe, D., et al. (2012). Small-molecule ligands bind to a distinct pocket in Ras and inhibit SOS-mediated nucleotide exchange activity. *Proc. Natl. Acad. Sci. USA* **109**, 5299–5304.
- Min, J.-H., Yang, H., Ivan, M., Gertler, F., Kaelin, W.G., Jr., and Pavletich, N.P. (2002). Structure of an HIF-1alpha-pVHL complex: hydroxyproline recognition in signaling. *Science* **296**, 1886–1889.
- Morelli, X., Bourgeas, R., and Roche, P. (2011). Chemical and structural lessons from recent successes in protein-protein interaction inhibition (2P2I). *Curr. Opin. Chem. Biol.* **15**, 475–481.
- Mortenson, P.N., and Murray, C.W. (2011). Assessing the lipophilicity of fragments and early hits. *J. Comput. Aided Mol. Des.* **25**, 663–667.
- Murray, C.W., and Verdonk, M.L. (2002). The consequences of translational and rotational entropy lost by small molecules on binding to proteins. *J. Comput. Aided Mol. Des.* **16**, 741–753.
- Murray, C.W., and Rees, D.C. (2009). The rise of fragment-based drug discovery. *Nat. Chem.* **1**, 187–192.
- Murray, C.W., Verdonk, M.L., and Rees, D.C. (2012). Experiences in fragment-based drug discovery. *Trends Pharmacol. Sci.* **33**, 224–232.
- Nazaré, M., Matter, H., Will, D.W., Wagner, M., Urmann, M., Czech, J., Schreuder, H., Bauer, A., Ritter, K., and Wehner, V. (2012). Fragment deconstruction of small, potent factor Xa inhibitors: exploring the superadditivity energetics of fragment linking in protein-ligand complexes. *Angew. Chem. Int. Edit. Engl.* **51**, 905–911.
- Page, M.I., and Jencks, W.P. (1971). Entropic contributions to rate accelerations in enzymic and intramolecular reactions and the chelate effect. *Proc. Natl. Acad. Sci. USA* **68**, 1678–1683.
- Petros, A.M., Dinges, J., Augeri, D.J., Baumeister, S.A., Betebenner, D.A., Bures, M.G., Elmore, S.W., Hajduk, P.J., Joseph, M.K., Landis, S.K., et al. (2006). Discovery of a potent inhibitor of the antiapoptotic protein Bcl-xL from NMR and parallel synthesis. *J. Med. Chem.* **49**, 656–663.
- Saxty, G., Woodhead, S.J., Berdini, V., Davies, T.G., Verdonk, M.L., Wyatt, P.G., Boyle, R.G., Barford, D., Downham, R., Garrett, M.D., and Carr, R.A. (2007). Identification of inhibitors of protein kinase B using fragment-based lead discovery. *J. Med. Chem.* **50**, 2293–2296.
- Stout, T.J., Sage, C.R., and Stroud, R.M. (1998). The additivity of substrate fragments in enzyme-ligand binding. *Structure* **6**, 839–848.
- Sun, Q., Burke, J.P., Phan, J., Burns, M.C., Olejniczak, E.T., Waterson, A.G., Lee, T., Rossanese, O.W., and Fesik, S.W. (2012). Discovery of small molecules that bind to K-Ras and inhibit Sos-mediated activation. *Angew. Chem. Int. Edit. Engl.* **51**, 6140–6143.
- Surade, S., and Blundell, T.L. (2012). Structural biology and drug discovery of difficult targets: the limits of ligandability. *Chem. Biol.* **19**, 42–50.
- Śledź, P., Stubbs, C.J., Lang, S., Yang, Y.-Q., McKenzie, G.J., Venkitaraman, A.R., Hyvönen, M., and Abell, C. (2011). From crystal packing to molecular recognition: prediction and discovery of a binding site on the surface of polo-like kinase 1. *Angew. Chem. Int. Edit. Engl.* **50**, 4003–4006.
- Teotico, D.G., Babaoglu, K., Rocklin, G.J., Ferreira, R.S., Giannetti, A.M., and Shoichet, B.K. (2009). Docking for fragment inhibitors of AmpC beta-lactamase. *Proc. Natl. Acad. Sci. USA* **106**, 7455–7460.
- Tsao, D.H.H., Sutherland, A.G., Jennings, L.D., Li, Y., Rush, T.S., 3rd, Alvarez, J.C., Ding, W., Dushin, E.G., Dushin, R.G., Haney, S.A., et al. (2006). Discovery of novel inhibitors of the ZipA/FtsZ complex by NMR fragment screening coupled with structure-based design. *Bioorg. Med. Chem.* **14**, 7953–7961.
- Wells, J.A., and McClendon, C.L. (2007). Reaching for high-hanging fruit in drug discovery at protein-protein interfaces. *Nature* **450**, 1001–1009.
- Yin, H., and Hamilton, A.D. (2005). Strategies for targeting protein-protein interactions with synthetic agents. *Angew. Chem. Int. Edit. Engl.* **44**, 4130–4163.